Title

# Identification of NeuN immunopositive cells in the adult mouse subventricular zone

Authors

Kengo Saito[1], Taro Koike[2], Fumiaki Kawashima[1], Hirofumi Kurata[1,3], Taku Shibuya[4], Takemasa Satoh[5], Yoshio Hata[4, 5], Hisao Yamada[2], Tetsuji Mori[1]

Affiliations

[1]Department of Biological Regulation, School of Health Science, Faculty of Medicine, Tottori University, Yonago, Tottori 683-8503, Japan

[2]Department of Anatomy and Cell Science, Kansai Medical University, Hirakata, Osaka, 573-1010, Japan

[3]Division of Child Neurology, Department of Brain and Neurosciences, Faculty of Medicine, Tottori University, Yonago, Tottori 683-8504, Japan

[4]Division of Integrative Bioscience, Institute of Regenerative Medicine and Biofunction, Tottori University Graduate School of Medical Sciences, Yonago, 683-8503, Japan.

[5]Division of Neurobiology, School of Life Sciences, Faculty of Medicine, Tottori University Yonago, 683-8503, Japan.

Abbreviated title

NeuN immunopositive cells in the adult SVZ

Associate Editor

Professor John Rubenstein

Key words

Adult neurogenesis, subventricular zone, neurogenic niche, heterogeneity, NeuN (RRID:AB_2298772 and RRID:AB_2532109)

Corresponding author

Tetsuji Mori

Department of Biological Regulation, School of Health Science, Faculty of Medicine, Tottori University, Nishi-Cho 86, Yonago, Tottori 683-8503, Japan

Phone and Fax: +81-859-38-6352

E-mail: mori-te@med.tottori-u.ac.jp

Grant information

This work was supported by JSPS KAKENHI Grant-in-Aid for Scientific Research(C), Grant

Number: 25430044 and 18K06830.

Abstract

In the adult rodent subventricular zone (SVZ), there are neural stem cells (NSCs) and the specialized neurogenic niche is critical to maintain their stemness. . To date, many cellular and non-cellular factors that compose the neurogenic niche and markers to identify subpopulations of Type A cells have been confirmed. In particular, neurotransmitters regulate adult neurogenesis and mature neurons in the SVZ have been only partially analyzed. Moreover, Type A cells, descendants of NSCs, are highly heterogeneous and more molecular markers are still needed to identify them. In the present study, we systematically classified NeuN, commonly used as a marker of mature and immature post-mitotic neurons, immunopositive (+) cells within the adult mouse SVZ. These SVZ-NeuN+ cells (SVZ-Ns) were mainly classified into two types. One was mature SVZ-Ns (M-SVZ-Ns). Neurochemical properties of M-SVZ-Ns were similar to those of striatal neurons, but their birth date and morphology were different. M-SVZ-Ns were generated during embryonic and early postnatal stages with bipolar peaks, and extended their processes along the wall of the lateral ventricle. The second type was small SVZ-Ns (S-SVZ-Ns) with features of Type A cells. They expressed not only markers of Type A cells, but also proliferated and migrated from the SVZ to the olfactory bulb. Furthermore, S-SVZ-Ns could be classified into two types by their spatial locations and glutamic acid decarboxylase 67 expression. Our data indicate that M-SVZ-Ns are a new component of the neurogenic niche and S-SVZ-Ns are newly identified subpopulations of Type A cells.

## Introduction

In the postnatal and adult mammalian brain, neurogenesis persists actively in the subgranular zone of the hippocampus and the subventricular zone (SVZ) lining the lateral ventricle (Lim and Alvarez-Buylla, 2016). In both regions, adult neural stem cells (NSCs) possess astrocyte-like features expressing glial fibrillary acid protein (GFAP). Three types of neural progenitor cells (NPCs) reside in the SVZ: GFAP immunopositive (+) NSCs (Type B cells) slowly proliferate and sequentially differentiate into fast-proliferating transient-amplifying cells (Type C cells expressing epidermal growth factor receptor, EGFR) and Type A cells. Type A cells expressing doublecortin (DCX) and polysialylated neural cell adhesion molecule (PSA-NCAM), divide several times, and migrate toward the olfactory bulb (OB) through the glial tube of the rostral migratory stream (RMS). They subsequently differentiate into a variety of OB interneurons, but mainly into GABAergic granule neurons (Lim and Alvarez-Buylla, 2016).

“Stemness,” such as proliferation and differentiation potential, of NSCs is maintained only

in the neurogenic regions of the adult brain, and neurogenesis is strictly regulated. To maintain stemness and regulate neurogenesis, both cell-intrinsic and extrinsic factors are necessary. Many extrinsic factors have been reported in the adult brain and construct the neurogenic niche; vasculature, microglia, ependymal cells, extracellular matrix, growth factors, cerebrospinal fluid (CSF), and neurotransmitters (Lim and Alvarez-Buylla, 2016). Neurotransmitters are important for the regulation of proliferation and migration of NPCs (Young et al., 2011).

In the striatum, 90-95% of neurons are medium-sized spiny neurons (MSNs); they are projection neurons expressing GABA and DARPP-32 (Ouimet et al., 1998; Reiner et al., 1998). The rest (5-10%) are interneurons with heterogeneous neurochemical properties, including GABAergic and cholinergic neurons (Kawaguchi et al., 1995). GABAergic interneurons are classified into three subtypes; 1) Parvalbumin (PV)+, 2) Calretinin (CR)+ and 3) neuronal Nitric oxide synthase (nNOS) / Somatostatin / Neuropeptide Y+ (Kawaguchi et al., 1995). Cholinergic interneurons are a distinct population from GABAergic interneurons (Kawaguchi et al., 1995). GABA-A receptors are expressed in Type A and B cells, and adult neurogenesis is regulated in an inhibitory manner by GABA (Bolteus and Bordey, 2004; Liu et al., 2005; Platel et al., 2008; Alfonso et al., 2012; Young et al., 2014). Nitric oxide (NO) also inhibits, but acetylcholine enhances adult neurogenesis (Moreno-López et al., 2004; Kaneko et al., 2006; Paez-Gonzalez et al., 2014). The sources of these neurotransmitters are complex. GABA is released from striatal GABAergic neurons and Type A cells (Bolteus and Bordey, 2004; Liu et al., 2005; Young et al., 2014). Some nitrergic neurons exist within the SVZ (Moreno-López et al., 2000; Romero-Grimaldi et al., 2008). Recently, Paez-Gonzalez et al. reported that cholinergic neurons reside within the “SVZ niche.” Unfortunately, they did not precisely define the “SVZ niche,” and their analysis included striatal cholinergic neurons residing close to the SVZ (Paez-Gonzalez et al., 2014). It is important to clarify the sources of neurotransmitters regulating adult neurogenesis, and it is still unclear whether there are other types of mature neurons within the SVZ.

CSF is also important for the regulation of adult neurogenesis. Migration of Type A cells is directed by the flow of CSF (Sawamoto et al., 2006). Type B cells have a cilium extending between ependymal cells and make a direct contact with CSF (Mirzadeh et al., 2008). Those cilia make synapses with serotonergic axons derived from the raphe nuclei on the surface of the lateral ventricle wall (Tong et al., 2014). It is noteworthy that CSF-contacting neurons (CSF-cNs) exist around the medullospinal central canal (they have processes or cilia that contact CSF) (Vígh et al., 2004). It is thought that CSF-cNs monitor contents of CSF: for example, pH, concentration of ions, hormones, and other factors, and perform non-synaptic transmission. More CSF-cNs are distributed in the caudal part than the anterior part in the medullospinal regions (Orts-Del’Immagine et al., 2016), and there is no clear evidence showing the existence of CSF-cNs in the wall of the lateral ventricles in higher vertebrates.

The classification of NPCs in the SVZ-RMS-OB system described above is a simplified model. Indeed, evidence has shown that each progenitor type contains several subpopulations (Merkle et al., 2007, 2014). Because a detailed classification of NPCs is still required, the number of marker molecules is still limited.

To identify mature neurons, the NeuN antibody is commonly used (Mullen et al., 1992). However, several lines of evidence indicate that some immature or progenitor cells express NeuN. In the developing central nervous system, the ventricular zone is principally devoid of NeuN expression (Mullen et al., 1992), but a few scattered post-mitotic and premigratory cells are NeuN+ in the developing human ventricular zone (Sarnat et al., 1998). Also, in the adult rodent brain, NeuN is transiently expressed in post-mitotic immature neurons in the hippocampus and OB (Seki, 2002; Brandt et al., 2003; Brown et al., 2003).

In the present study, we systematically analyzed and characterized NeuN+ mature neurons within the SVZ, and termed them M-SVZ-Ns (mature SVZ-NeuN+ cells) to discriminate them from the striatal neurons. Interestingly, we found that some Type A cells were also NeuN+. Because they had small nuclei, we termed them S-SVZ-Ns (small SVZ-NeuN+ cells).

## Materials and Methods

### Animals

Eight timed-pregnant ICR mice were used for analysis of the embryonic brain. The day when a vaginal plug was detected was defined as embryonic day (E) 0. For analysis of the adult brain, ten six-week-old male ICR mice (RRID:MGI:5462094) were used. ICR mice were supplied by Japan SLC. Inc. (Hamamatsu, Japan). Also, in some experiments, three six-week-old GAD (glutamic acid decarboxylase) 67-GFP Knock-In mice (RRID:IMSR_RBRC03674) (Tamamaki et al., 2003) including one male and two females were used. The GAD67-GFP mouse strain was provided by RIKEN BRC through the National Bio-Resource Project of the MEXT, Japan. They were maintained under the C57/BL6 background. All experiments were performed in compliance with the Guidelines for Animal Experimentation, Faculty of Medicine, Tottori University under the International Guiding Principles for Biomedical Research Involving Animals. Animals were housed in standard cages with ad libitum access to food and water.

### BrdU labeling

In the rat, striatal neurons are generated between E12 to postnatal day (P) 5 (Marchand and Lajoie, 1986; Wright et al., 2013). To label and chase proliferating cells at E11, 12, 13, 16, 18, and P1, 3, 7 , 5-bromo-2’-deoxyuridine (BrdU, Tokyo Kasei, Tokyo, Japan) was injected intraperitoneally (ip) at a dose of 50 mg/kg. BrdU was dissolved in

phosphate-buffered saline (PBS) at 10 mg/ml. All BrdU-received mice were analyzed at six weeks old. To label adult NPCs, BrdU was injected three times at an interval of two hours, and analyzed three hours or seven days after the last injection of BrdU.

Intracellular injection of Lucifer Yellow

Using lightly fixed thick brain slices, the fluorescent dye Lucifer Yellow (LY, Thermo Fisher Scientific, Waltham, MA, USA) was injected into single cells under an epi-fluorescence microscope (Oga et al., 2017). Mice were deeply anesthetized by pentobarbital (50 mg/kg, ip), perfused transcardially with PBS, followed by 4% formaldehyde (FA) in PBS at a volume equal to animal weight, and post-fixed with the same fixative for three hours. Coronal sections (200 μm thick) were cut by a microslicer (DTK-1000, Dosaka EM, Kyoto, Japan). To visualize nuclei, tissues were incubated with 1 μg/ml of Hoechst33258 (Sigma, St Louis, MO, USA) in PBS at room temperature for 15 min. Sections were set in a Petri dish filled with PBS under a fixed-stage epi-fluorescence microscope (Axioskop-FS, Zeiss, Oberkochen, Germany) equipped with a V-2A filter block (EX 380-420, DM 430, BA 450, Nikon, Tokyo, Japan) and a micromanipulator (MX-1, Narishige, Tokyo, Japan). A fine-tipped glass capillary (250~300 MΩ) was filled with 3% LY in 0.05M Tris buffer pH 8.4, and LY was injected with continuous current (~20 nA, Union-200 Iontophoresis Pump, Kation Scientific, Minneapolis, MN, USA). After LY injection, the section was post-fixed with 4% FA in PBS overnight.

Retrograde axonal tracing

FluoroGold (FG, Hydroxystilbamidine, Abcam, Cambridge, UK) was dissolved in 0.9% NaCl at 2%. Adult mice are anesthetized with pentobarbital (50 mg/kg, ip) and placed in a stereotaxic apparatus. Each mouse received a unilateral injection of 0.1 μl of FG into the lateral globus pallidus (LGP, coordinates: -0.4 mm caudal, 2.0 mm lateral from the bregma, 3.5 mm depth from the surface of the brain), the medial globus pallidus (MGP, coordinates: -1.3 mm caudal, 1.8 mm lateral from the bregma, 4.0 mm depth from the surface of the brain) and the substantia nigra (SN, coordinates: -3.1 mm caudal, 1.2 mm lateral from the bregma, 4.1 mm depth from the surface of the brain) with a fine-tipped glass capillary that had a 5-min waiting period before withdrawal. Three days after the FG injection, mice were analyzed. To visualize nuclei, sections were stained with 0.04 μg/ml of propidium iodide (PI, Thermo Fisher Scientific) solution. Stereotaxis coordinates are based on those of Paxinos and Franklin (Paxinos and Franklin, 2001).

Tissue preparation for immunohistochemistry

For histological analysis, mice were perfused with 4% FA in PBS as described above. The brains were removed and post-fixed with 4% FA in PBS overnight. All brains were

cryoprotected with 20% sucrose in PBS, embedded in Super CryoMount (Muto Pure Chemicals, Tokyo, Japan), snap frozen on dry ice, and cut transversely using a cryostat. Coronal sections were made as 30 μm-thick free-floating sections.

Primary antibody characterization

The primary antibodies used in this study are listed in Table 1.

The anti-BrdU antibody (Abcam; Cat. # ab6326, RRID:AB_305426) recognizes BrdU, but not thymidine (Aten et al., 1992). We confirmed that this antibody did not stain any brain section that did not receive BrdU.

With the anti-Calretinin antibody (Frontier Institute, Hokkaido, Japan; Cat. # Calretinin-Rb-Af200, RRID:AB_2571666), immunoblot detects a single band at 30 kDa from mouse brain lysate (manufacturer's information). With this antibody, we obtained a similar immuno-staining pattern as a previous study (Merkle et al., 2007).

The anti-activated Caspase-3 (Cas3) antibody (Promega, Madison, WI, USA; Cat. # G748A, RRID:AB_430875) specifically recognizes TUNEL-positive apoptotic cells (Goodyear et al., 2014). In the present study, Cas3 antibody stained only pyknotic nuclei determined by Hoechst33258 staining.

With the anti-choline acetyltransferase (ChAT) antibody (Millipore, Temecula, CA, USA; Cat. # AB144P, RRID:AB_11214092), immunoblot detects a single band at ~68-70 kDa from NIH/3T3 lysate (manufacturer's information). With this antibody, we obtained a similar staining pattern as a previous studies(Mori et al., 2004; Kaneko et al., 2006).

The anti-DARPP-32 antibody (Abcam; Cat. # ab40801, RRID:AB_731843) recognizes a single band at 32 kDa on western blotting of rat and mouse brain lysate, and this antibody can be absorbed by blocking peptide (manufacturer's information). With this antibody, we obtained a similar staining pattern as previous studies (Ouimet et al., 1998; Reiner et al., 1998).

The goat anti-doublecortin (DCX) antibody (Santa Cruz Biotechnology, Santa Cruz, CA, USA; Cat. # sc8066, RRID:AB 2088494) detects a single band at 45 kDa on western blotting of adult rat olfactory bulb lysate (Brown et al., 2003). The guinea pig anti-DCX antibody (Millipore; Cat. # AB2253, RRID:AB_10014654) recognizes a protein at ~45 kDa on western blotting of rat and ferret brain lysate (manufacturer's information) (Takamori et al., 2014). With these two anti-DCX antibodies, we obtained similar staining patterns between them and as a previous study (Brandt et al., 2003).

The anti-EGFR antibody (Millipore, #06-129, RRID:AB_2314360) detects a single band at 170 kDa on western blotting of A431 human carcinoma cell line lysate (manufacturer's information). With this antibody, we obtained a similar staining pattern as previous studies (Romero-Grimaldi et al., 2008; Mori et al., 2012).

The anti-green fluorescent protein (GFP) antibody (MBL, Aichi, Japan; Cat. # 598,

RRID:AB_591816) recognizes a protein on western blotting of GFP fusion protein-transfected cells, but not of parental cells (manufacturer's information). This antibody did not stain any cells in wild-type brain sections, but a specific signal was detected in GABAergic neurons in GAD67-GFP mouse sections.

The anti-HuC/D antibody (Thermo Fisher Scientific, Waltham, MA, USA; Cat. # A-21271, RRID:AB_221448) recognizes Elav RNA binding protein family members, HuC, HuD and Hel-N1, and stained immature and mature neurons (Graus and Ferrer, 1990; Marusich et al., 1994). The antibody specificity was confirmed by blocking peptide with the HuD peptide (Marusich et al., 1994). Cellular localization of the HuC/D signal was different between NPCs and mature neurons; mainly in the cytoplasm and nucleus, respectively (Okano and Darnell, 1997; Wang et al., 2015). With this antibody, we obtained a similar staining pattern as previous studies (Graus and Ferrer, 1990; Marusich et al., 1994).

The anti-MCM2 antibody (Santa Cruz Biotechnology; Cat. # sc-9839, RRID:AB_648841) recognizes a 127 kDa band in the nuclear extract of HeLa cells and reacts to MCM2 of rat, mouse, and human origin by western blotting (manufacturer's information). This antibody was used to detect proliferating cells in the adult SVZ by double-immunostaining with thymidine analogues, and we obtained a similar staining pattern as a previous study (Maslov et al., 2004).

The mouse NeuN antibody (Millipore; Cat. # MAB377, RRID:AB_2298772) detects two to three bands in the 45-50 kDa range on western blotting of whole-cell or nuclear extract lysate of mouse brain (manufacturer's information). The rabbit NeuN antibody (Abcam; Cat. # ab177487, RRID:AB_2532109) detects two bands in the 46-50kDa on western blotting of mouse brain lysate (manufacturer's information). These antibodies recognize a splicing factor Fox-3 (Kim et al., 2011) and label the majority of mature neurons, with some exceptions, such as mitral cells of the OB and Purkinje cells (Mullen et al., 1992). We obtained a similar staining pattern as a previous study (Mullen et al., 1992), and signals obtained with these antibodies completely overlapped (data not shown).

The anti-nNOS antibody (Frontier Institute; Cat. # nNOS-Rb-Af480, RRID:AB_2571815) recognizes a protein at ~150 kDa on western blotting from mouse tissue. This antibody stains Somatostatin-expressing interneurons in the mouse striatum (manufacturer's information). With this antibody, we obtained a similar staining pattern as a previous study (Kawaguchi et al., 1995).

The anti-Parvalbumin antibody (Frontier Institute; Cat. # PV-Rb-Af750, RRID:AB_2571613) recognizes a protein at 16 kDa on western blotting from mouse tissue (Nakamura et al., 2004). This antibody selectively stains subpopulations of interneurons as well as cerebellar Purkinje cells (manufacturer's information). With this antibody, we obtained a similar staining pattern as a previous study (Kawaguchi et al., 1995).

The anti-Sox2 antibody (Millipore; Cat. # AB5603, RRID:AB_2286686) recognizes a protein

at 34 kDa on western blotting from mouse and human cell lines (manufacturer's information). This antibody stains NPCs in the adult mouse neurogenic region, and we obtained a similar staining pattern as a previous study (Lagace et al., 2007).

Immunohistochemistry

Immunohistochemical analysis was performed as follows: the sections were incubated with primary antibodies in PBS containing 0.3% Triton X-100 (0.3% PBST) at 4°C overnight; washed three times in PBS; and incubated with species-specific donkey secondary antibodies in 0.3% PBST at 4°C for two hours. Secondary antibodies used in this study were Cy2 labeled donkey anti-goat IgG (1:200, Jackson ImmunoResearch, West Grove, PA, USA; Cat. # 705-225-147, RRID:AB_2307341), Cy2 labeled donkey anti-guinea pig IgG (1:200, Jackson ImmunoResearch; Cat. # 706-225-148, RRID:AB_2340467), Cy2 labeled donkey anti-rat IgG (1:200, Jackson ImmunoResearch; Cat. # 712-225-153, RRID:AB_2340674), Cy3 labeled donkey anti-mouse IgG (1:200, Jackson ImmunoResearch; Cat. # 715-165-151, RRID:AB_2315777), Cy3 labeled donkey anti-sheep IgG (1:200, Jackson ImmunoResearch; Cat. # 713-165-147, RRID:AB_2315778), Cy5 labeled donkey anti-goat IgG (1:200, Jackson ImmunoResearch; Cat. # 705-175-147, RRID:AB_2340415), AlexaFluor488 labeled donkey anti-mouse IgG (1:800, Thermo Fisher Scientific; Cat # A-21206, RRID:AB_2535792), and AlexaFluor488 labeled donkey anti-rabbit IgG (1:800, Thermo Fisher Scientific; Cat # A-21202, RRID:AB_141607). After incubation, the sections were washed three times in PBS, mounted on glass slides, and coverslipped with mounting media containing 50% glycerol, 5 µg/ml Hoechst33258 (Sigma), and 0.2% n-propyl gallate in PBS. For double immunostaining, the sections were incubated in a primary antibody cocktail, and then in a secondary antibody cocktail.

To detect BrdU-labeled cells, the sections were incubated in 2M HCl at 27°C for 30 min, neutralized in 0.1M sodium borate (pH 8.5) for 30 min, and washed three times in PBS before incubating with the anti-BrdU antibody. To detect the MCM2 antigen, sections were boiled in 10 mM sodium citrate buffer (pH 6.0) for 7 min followed by washing three times in PBS before incubating with the anti-MCM2 antibody.

Image acquisition and nuclear volume analysis

Images were acquired using a laser scanning confocal microscope (LSM 780, Zeiss). To acquire single optical images, optical section thickness was adjusted to 1 µm for each channel. Serial z-sectioning images were acquired and three-dimensional (3D) images were reconstructed using ZEN software (Zeiss; RRID:SCR_013672). For nuclear volume analysis, 3D nuclear images were reconstructed, and their volume was measured by Imaris software (Bitplane, Zurich, Switzerland; RRID:SCR_007370). Data are presented as the average ± standard deviation.

Electron microscopy analysis

Mice were transcardially perfused with 0.1% or 2% glutaraldehyde (GA)/4% FA in PBS. Brains were post-fixed with the same fixative overnight and cut into 50 μm-thick sections with a microslicer. Sections were pretreated with 0.1% PBST on ice for 30 min, afterwards Triton X-100 was excluded from all buffers. M-SVZ-Ns were visualized using immunostaining with the NeuN antibody in 2% GA/4% FA fixed brain sections, followed by the ABC reaction kit (Vectastain Elite ABC-HRP mouse IgG kit, Vevtor Laboratories, Burlingame, CA, US; Cat. # PK-6102, RRID:AB_2336821). A chromogenic reaction was performed with Nickel/DAB solution (0.05% of nickel chloride, 0.2 mg/ml of diaminobenzidine, 0.006% of $H_2O_2$ in 50 mM Tris, pH7.6). After sections were mounted on non-coating glass slides, images were acquired with a light microscope (Optiphot, Nikon) equipped with a digital camera (Eos Kiss X8i, Cannon, Tokyo, Japan). S-SVZ-Ns were visualized by immunofluorescent staining with NeuN and DCX in 0.1% GA/4% FA fixed brain sections. Fluorescent images were acquired with a laser scanning confocal microscope to confirm co-labeling by the NeuN and DCX antibodies.

Sections were recovered from glass slides and fixed with 1% $OsO_4$ on ice for two hours, followed by embedding in epoxy resin, and sectioning with an ultramicrotome. The sections were stained with 1% uranyl acetate for 15 min followed by Sato's lead staining solution for 5 min (Sato, 1968). Cells that were identified by immunostaining were observed with a transmission electron microscope (JEM-1400A, JEOL, Tokyo, Japan).

Quantification analysis

Quantifying immunopositive M-SVZ-Ns was manually performed at 400x magnification with an epi-fluorescence microscope (TE2000, Nikon). Quantification of BrdU and NeuN double positive striatal neurons was performed using particle analysis function of Image J (https://imagej.nih.gov/ij/, RRID:SCR_003070) on images obtained with an epi-fluorescence microscope (BZ-9000, Keyence, Osaka, Japan) at 200x magnification. The adult SVZ and striatum were analyzed at the anterior regions (anteroposterior 1.0 to 0 mm from the bregma). Every tenth 30-μm-thick section was collected, and a total of three sections were analyzed from each mouse. Three mice were analyzed from each group. Data are presented as the average ± standard deviation.

Statistical analysis

Statistical analysis was performed using R software (http://www.r-project.org/, RRID:SCR_001905). The level of significance was determined using a one-way ANOVA followed by Tukey's post hoc test or student's *t*-test. Statistical significance was set at $p<0.05$.

## Results

### Identification of NeuN+ cells in the adult SVZ

We identified NeuN+ cells within the SVZ (SVZ-NeuN+ cells, SVZ-Ns). Although there were many NeuN+ neurons close to the SVZ, we analyzed NeuN+ cells when more than half of their nuclei were embedded in the SVZ (Fig. 1). They were classified into two types. One had a round and large nucleus, a typical morphology of mature neurons (Fig. 1b-d), and the other had a small nucleus (Fig.1 c-d). It was notable that only the latter cells expressed DCX (Fig. 1c-d). According to the nucleus morphology and DCX expression, we termed them mature-SVZ-Ns (M-SVZ-Ns) and small-SVZ-Ns (S-SVZ-N).

The number of M-SVZ-Ns in each section was very small, and they were scattered relatively evenly throughout the SVZ. In most cases, M-SVZ-Ns localized very close to the wall of the lateral ventricle in the middle part of the SVZ (Fig. 1b).

In contrast, S-SVZ-Ns resided in the dorsal and ventral parts of the SVZ and were absent from middle part of the SVZ. Thus, we further classified them into dorsal S-SVZ-Ns (DS-SVZ-Ns, Fig. 1c) and ventral S-SVZ-Ns (VS-SVZ-Ns, Fig. 1d).

Next, we analyzed the nuclear morphologies of SVZ-Ns in the 3D reconstructed confocal microscopy images. The nuclear volume of the M-SVZ-Ns was not significantly different from that of the striatal neurons, but was significantly larger than that of the DS- and VS-SVZ-Ns (Fig, 1e). Interestingly, the nuclear morphology of the DS-SVZ-Ns was significantly elongated when the ratio of the longest diameter to the shortest diameter of their nuclei was calculated (Fig. 1f).

M-SVZ-Ns were also devoid of GFAP and EGFR immunoreacitivity, and they were enwrapped by GFAP+ and EGFR+ processes (Fig. 2a-b). In the present study, we analyzed anterior SVZ (anterior from the bregma) of the adult brain, but M-SVZ-Ns were also found in the caudal SVZ (Fig. 3c). Moreover, in the early postnatal brain, M-SVZ-Ns without expressing DCX (Fig. 2d) and S-SVZ-Ns expressing DCX (Fig. 2e) were detected.

### Characterization of M-SVZ-Ns

#### Classification of M-SVZ-Ns

To characterize M-SVZ-Ns, we classified them with neuronal markers. First, we quantified the number of M-SVZ-Ns. The average number of M-SVZ-Ns was approximately 70 cells per section (Fig. 3a). Cytoplasmic HuC/D, a neuronal marker, + cells with small nuclei expressed Sox2, a marker of NPCs, but nuclear HuC/D+ cells with large nuclei did not express Sox2 (Fig. 3b). Thus, we quantified only HuC/D+ cells with nuclear staining. The average number of HuC/D+ neurons in the SVZ was approximately 12 per section and was significantly fewer

than that of NeuN+ cells (Fig. 3a). In fact, there were many HuC/D immunonegative (-) cells among NeuN+ cells in the SVZ (Fig. 3c).

Second, we classified M-SVZ-Ns with striatal neuron markers. Because the striatum is adjacent to the SVZ, we supposed that M-SVZ-Ns have similar phenotypes with the striatal neurons. Thus, we examined expressions of GAD67, a GABAergic neuron marker, and DARPP-32. To facilitate identification of GAD67+ neurons, we used GAD67-GFP knock-in mice. As a result, approximately 94% and 83% of M-SVZ-Ns were GFP+ and DARPP-32+, respectively (Figs. 3d-f). All DARPP-32+ cells in the SVZ were NeuN+ in the SVZ (data not shown). Next, we examined the interneuron markers including nNOS, CR, PV, and ChAT. Approximately 5%, 4%, and 2% of M-SVZ-Ns were nNOS+, CR+, and PV+, respectively (Figs. 3d, 3g-i). As for cholinergic neurons, extremely few M-SVZ-Ns were ChAT+ (Fig. 3d). When we analyzed sixteen sections from three mice, only one ChAT+ M-SVZ-N was identified (Fig. 3j); although, there were some ChAT+ cells very close to the SVZ. ChAT+ processes were abundant in the striatum, but they made a clear boundary with SVZ cells as described previously (Kaneko et al., 2006) (data not shown). In contrast, many nNOS+ processes intruded into the SVZ as described previously (Moreno-López et al., 2000; Romero-Grimaldi et al., 2008) (data not shown). Interestingly, M-SVZ-Ns extended their processes along the wall of the lateral ventricle (Fig. 3g, 3i-j).

Birth date analysis of M-SVZ-Ns

To determine the birth date of M-SVZ-Ns, we injected BrdU in the timed-pregnant mice or postnatal pups and analyzed them in the adult stage. We found that M-SVZ-Ns were generated from E11 to P3 with bipolar peaks at E13 and P1. After P1, dramatically fewer M-SVZ-Ns were generated, and we could not identify M-SVZ-Ns generated after P7 (Fig. 4a, c). In contrast, vast majority of striatal neurons were generated during embryonic stages with a peak around E13 and very small number of striatal neurons were generated during postnatal stages (Fig. 4b). This data supports previous studies (Bayer, 1984; Marchand and Lajoie, 1986; Wright et al., 2013).

Morphology of M-SVZ-Ns

As described above, the morphology of some M-SVZ-Ns was partially revealed (Fig. 3g, 3i-j). To further elucidate the entire morphology of M-SVZ-Ns, we performed an intracellular injection of Lucifer Yellow (LY). Many processes of M-SVZ-Ns ran through the parenchyma of the striatum almost parallel to the wall of the lateral ventricle (Fig. 5a). In particular, some of them ran long distance on the surface or within the SVZ (Fig. 5b-c). The ovaral morphology of M-SVZ-Ns was flat. On the other hand, the dendrites of typical MSNs branched radially (Fig. 5c, inset).

Electron microscopy analysis of M-SVZ-Ns indicated that they had a typical neuronal

morphology with a large and round nucleus, a nuclear body (Fig. 5d), abundant rough endoplasmic reticulum, free ribosomes and mitochondria, and synapses (data now shown). M-SVZ-Ns made close contact with ependymal cells, but they did not have any processes or cilia contacting CSF (Fig. 5d).

Axonal target of M-SVZ-Ns

From marker expression analysis, it was supposed that DARPP-32+ M-SVZ-Ns might project their axons to the same target sites with MSNs, such as the lateral and medial globus pallidus (LGP and MGP) and substantia nigra (SN) (Crittenden and Graybiel, 2011). Thus, we injected fluorescent retrograde axon tracer, FluoroGold (FG), in the MGP, LGP, and SN. In each experiment, some somata of M-SVZ-Ns were labeled by FG (Fig. 5e and data not shown).

Characterization of S-SVZ-Ns

Proliferation and migration of S-SVZ-Ns

Because S-SVZ-Ns expressed DCX, they could be a subtype of Type A cells. To further confirm that S-SVZ-Ns were NPCs, we performed double immunostaining with anti-NeuN and anti-Sox2 antibodies. Virtually all S-SVZ-Ns were Sox2+ (Fig. 6a-b). Furthermore, S-SVZ-Ns expressed MCM2, a marker of proliferating cells, but did not express IbaI or GFAP (Fig. 6c-d and data not shown). Thus, we labeled and chased proliferating cells in the adult SVZ by pulse injections of BrdU. Three hours after the last injection of BrdU, there were a few NeuN+/DCX+/BrdU+ cells in the SVZ (Fig. 7a), but not in the OB (Fig. 7b). In contrast, one week after the last injection of BrdU, we detected many NeuN+/DCX+/BrdU+ cells in the OB (Fig. 7c).

These results in the SVZ were in sharp contrast to those in the hippocampus. There were many NeuN+/DCX+ cells in the subgranular zone, but those cells never expressed MCM2 (data not shown). These results in the hippocampus support the data reported by other research groups (Seki, 2002; Brandt et al., 2003; Brown et al., 2003).

Heterogeneity of S-SVZ-Ns

Interestingly, we found that GFP was expressed in the VS-SVZ-Ns, but not in the DS-SVZ-Ns in GAD67-GFP mice (Fig. 8a-b). Although there were both NeuN+/DCX+/GFP+ cells and NeuN+/DCX+/GFP- cells in the RMS (Fig. 8c), we identified only NeuN+/DCX+/GFP+ cells in the OB (Fig. 8d). There are two possibilities: 1) NeuN+/DCX+/GFP- cells began to express GFP during migration, or 2) they were eliminated by apoptosis. It has been reported that nearly half of newly generated cells undergo cell death (Biebl et al., 2000). To discriminate between these possibilities, we performed double immunostaining with the NeuN and anti-activated Caspase-3 (Cas3) antibodies. Virtually no

NeuN+ cells with small nuclei were Cas3+ in the RMS (Fig. 9a).

To further characterize S-SVZ-Ns, we performed electron microscopy analysis. Although S-SVZ-Ns were NeuN+, their morphology was clearly different from that of mature neurons. S-SVZ-Ns had scant cytoplasm and lax chromatin (Fig. 9b).

## Discussion

In this study, we identified two new cell-populations labeled by the NeuN antibody in the adult SVZ. One was M-SVZ-N, which were mature neurons in the SVZ. M-SVZ-Ns were similar to striatal neurons in neurochemical properties, but different in their birth dates and morphologies. The other was S-SVZ-N, which were subpopulations of Type A cells. Mature neurons in the SVZ have been partially analyzed, but we analyzed them systematically for the first time. And S-SVZ-Ns were newly identified cell populations.

### M-SVZ-Ns are a new component of the neurogenic niche in the adult SVZ.

Our analysis revealed that the composition of markers for M-SVZ-Ns was similar to that of striatal neurons (Kawaguchi et al., 1995; Reiner et al., 1998). Furthermore, projection neuron type M-SVZ-Ns shared the axonal target nuclei with MSNs, such as LGP, MGP, and SN (Crittenden and Graybiel, 2011). Indeed, M-SVZ-Ns might be a subtype of striatal neurons. Although the SVZ and striatum locate next to each other, they have completely different functions. Thus, M-SVZ-Ns and striatal neurons could have different functions. In fact, the birth dates and morphologies of M-SVZ-Ns were different from the striatal neurons. The striatum is compartmentalized with neurochemically defined structures, the patch and matrix, and patch neurons are generated earlier (E12-16) than matrix neurons (E17-20) in the rat brain (van der Kooy and Fishell, 1987; Fishell and van der Kooy, 1991). M-SVZ-Ns were generated during embryonic and postnatal periods with peaks at E13 and P1. This result suggests that there could be patch/matrix-like compartments within the M-SVZ-Ns. An intracellular injection of LY revealed the entire morphology of the M-SVZ-Ns. They extended some processes on the surface or within the SVZ and seemed to contact many NPCs. Electron microscopy analysis revealed that M-SVZ-Ns had synapses. Thus, there is a possibility that M-SVZ-Ns form a neural circuit within the SVZ and integrate the signals from neurons outside the SVZ to regulate adult neurogenesis (see below).

### M-SVZ-Ns might regulate adult neurogenesis by releasing neurotransmitters.

GABA and NO inhibit proliferation and migration of NPCs (Bolteus and Bordey, 2004; Liu et al., 2005; Platel et al., 2008; Alfonso et al., 2012; Young et al., 2014), but acetylcholine enhances proliferation and survival of NPCs (Mohapel et al., 2005; Kaneko et al., 2006;

Paez-Gonzalez et al., 2014). Thus, interneuron type M-SVZ-Ns could directly regulate adult neurogenesis by releasing these neurotransmitters. GABA seems to be the most important among them because the majority of M-SVZ-Ns were GABAergic neurons. In addition, Type A cells release GABA and abundant GABAergic striatal neurons exist close to the SVZ (Bolteus and Bordey, 2004; Liu et al., 2005; Young et al., 2014). Nitrergic neurons were the largest interneuron type M-SVZ-Ns, and many nNOS+ processes were detected within the SVZ (Moreno-López et al., 2000; Romero-Grimaldi et al., 2008); however, cholinergic M-SVZ-Ns were very few. Furthermore, ChAT+ processes made a clear boundary with SVZ cells. This result supports the data presented by Kaneko et al. (Kaneko et al., 2006), but conflicts with the data presented by Paez-Gonzalez et al. (Paez-Gonzalez et al., 2014). Because Paez-Gonzalez et al. used transgenic mice in which fluorescent protein is expressed in the cholinergic neurons, detection sensitivity could be higher than the immunohistochemistry.

Projection neuron type M-SVZ-N might form a closed circuit.

The effect of dopamine on adult neurogenesis is complex. Dopamine receptors are classified into two types: D1 type (D1 and D5) and D2 type (D2, D3 and D4). D2 receptors enhance proliferation of adult NPCs, but D1 receptors do not (O'Keeffe et al., 2009; Kim et al., 2010). GABAergic MSNs innervate to the dopaminergic projection neurons in the SN (Kawaguchi et al., 1995; Kawaguchi, 1997). It is known that D2 receptors are expressed in Type C cells, dopaminergic projection neurons in the SN innervate to the striatal neurons and Type C cells (Kawaguchi et al., 1995; O'Keeffe et al., 2009; Kim et al., 2010). In this study, some M-SVZ-Ns innervated to the SN. Thus, M-SVZ-Ns could form a closed circuit with dopaminergic neurons in the SN to regulate proliferation of NPCs. Another possibility is that because MSNs have many axon collaterals within the striatum (Kawaguchi, 1997), projection neuron type M-SVZ-Ns can also have axon collaterals to exert direct effects on NPCs.

M-SVZ-Ns did not have direct contact to CSF.

The anti-HuC/D antibody is used to detect mature neurons, but it can also label NPCs (Okano and Darnell, 1997; Wang et al., 2015). Interestingly, we found that the number of NeuN+ M-SVZ-Ns was much larger than that of HuC/D+ M-SVZ-Ns. Virtually all HuC/D+ cells with large nuclei were NeuN+, but many NeuN+ cells did not express HuC/D in the SVZ. CSF-cNs exhibit immature neuron properties; they weakly express NeuN, but also the immature neuron markers DCX, PSA-NCAM, and HuC/D (Marichal et al., 2009; Kútna et al., 2014; Orts-Del'Immagine et al., 2016). Importantly, maturity of CSF-cNs increases toward the anterior CNS. NeuN immunoreactivity increases from caudal to rostral regions, but HuC/D expression shows a tendency to decrease (Orts-Del'Immagine et al., 2016). The cell

bodies of some M-SVZ-Ns appeared to be positioned between ependymal cells. Thus, we supposed that M-SVZ-Ns were a subtype of CSF-CNs, or M-SVZ-Ns have cilia protruding between the ependymal cells and make synapses on the lateral ventricle surface, like Type B cells (Mirzadeh et al., 2008; Tong et al., 2014). However, our electron microscopy analysis revealed that M-SVZ-Ns were completely separated from the lateral ventricle by the ependymal cells.

S-SVZ-Ns were Type A cells.

S-SVZ-Ns expressed DCX, proliferated, and migrated. Moreover, they possessed fine structural properties of Type A cells (Doetsch et al., 1997). Thus, S-SVZ-Ns were Type A cells. Although there were many NeuN+/DCX+ cells in the adult hippocampus, they were post-mitotic.

Brown et al. described the small number of NeuN+/DCX+ cells in the OB, and they speculated that those cells were down-regulating DCX expression and differentiating into neurons (Brown et al., 2003). Unfortunately, Brown et al. did not further analyze those cells, they should correspond to S-SVZ-Ns in the OB. To the best of our knowledge, this study is the first report that subpopulations of proliferating Type A cells expressed NeuN in the SVZ and the RMS.

S-SVZ-Ns were heterogeneous.

NSCs in the SVZ produce a variety of OB interneurons and are heterogeneous in their differentiation potential. Their fates are determined by a spatial code during development (Merkle et al., 2007). Thus, Type A cells should also be heterogeneous (Nam et al., 2007). For example, neuronal features become apparent before their progenies reach their final destinations; GAD65/67 are already expressed in a subpopulation of Type A cells in the SVZ (De Marchis et al., 2004; Nam et al., 2007); and tyrosine hydroxylase begins to be expressed in young dopaminergic neurons migrating in the OB (Baker et al., 2001).

S-SVZ-Ns were further subdivided into DS-SVZ-Ns and VS-SVZ-Ns. Because virtually no S-SVZ-Ns expressed Cas3, DS-SVZ-Ns might upregulate GAD67 expression during migration, and DS-SVZ-Ns and VS-SVZ-Ns could be different populations possessing different spatial codes (Merkle et al., 2007). Thus, the NeuN antibody can identify new subpopulations of Type A cells. The NeuN antibody recognizes the splicing factor Fox-3, and the precise function of Fox-3 remains unclear (Kim et al., 2011). In addition, the function of Fox-3 in proliferating S-SVZ-Ns should be studied further.

Conclusion

In the present study, we identified M-SVZ-Ns within the SVZ and they were a new cellular component of the neurogenic niche. M-SVZ-Ns were similar to striatal neurons in neurochemical properties, but different in two points; morphology and birth date. In addition, we identified S-SVZ-Ns in the SVZ-RMS-OB system, which were newly identified subpopulations of Type A cells.

Acknowledgements

This research was partly performed at the Tottori Bio Frontier managed by the Tottori prefecture. This work was supported by JSPS KAKENHI Grant-in-Aid for Scientific Research(C), Grant Number: 25430044 and 18K06830.

Conflict of interest

All authors declare that no conflict of interest exists.

Role of authors

All authors had full access to all study data and take responsibility for the integrity of the data and the accuracy of the data analysis. Study concept and design: TM; Acquisition of data: KS, TK, FK, HK, TS, TS; Analysis and interpretation of data: KS, TK, HY; Drafting of the manuscript: TM; Critical revision of article for important intellectual content: YH, HY; Statistical analysis: KS; Obtained funding: TM; Study supervision: TM.

References

Alfonso J, Le Magueresse C, Zuccotti A, Khodosevich K, Monyer H. 2012. Diazepam binding inhibitor promotes progenitor proliferation in the postnatal SVZ by reducing GABA signaling. Cell Stem Cell 10:76–87.

Aten J a, Bakker PJ, Stap J, Boschman G a, Veenhof CH. 1992. DNA double labelling with IdUrd and CldUrd for spatial and temporal analysis of cell proliferation and DNA replication. Histochem J 24:251–259.

Baker H, Liu N, Chun HS, Saino S, Berlin R, Volpe B, Son JH. 2001. Phenotypic differentiation during migration of dopaminergic progenitor cells to the olfactory bulb. J Neurosci 21:8505–8513.

Bayer SA. 1984. Neurogenesis in the rat neostriatum. Int J Dev Neurosci 2:163–75.

Biebl M, Cooper CM, Winkler J, Kuhn HG. 2000. Analysis of neurogenesis and programmed cell death reveals a self-renewing capacity in the adult rat brain. Neurosci Lett 291:17–20.

Bolteus AJ, Bordey A. 2004. GABA release and uptake regulate neuronal precursor migration in the postnatal subventricular zone. J Neurosci 24:7623–7631.

Brandt MD, Jessberger S, Steiner B, Kronenberg G, Reuter K, Bick-Sander A, von der Behrens W, Kempermann G. 2003. Transient calretinin expression defines early postmitotic step of neuronal differentiation in adult hippocampal neurogenesis of mice. Mol Cell Neurosci 24:603–613.

Brown JP, Couillard-Després S, Cooper-Kuhn CM, Winkler J, Aigner L, Kuhn HG. 2003. Transient expression of doublecortin during adult neurogenesis. J Comp Neurol 467:1–10.

Crittenden JR, Graybiel AM. 2011. Basal Ganglia disorders associated with imbalances in the striatal striosome and matrix compartments. Front Neuroanat 5:59.

Doetsch F, García-Verdugo JM, Alvarez-Buylla A. 1997. Cellular composition and three-dimensional organization of the subventricular germinal zone in the adult mammalian brain. J Neurosci 17:5046–5061.

Fishell G, van der Kooy D. 1991. Pattern formation in the striatum: neurons with early projections to the substantia nigra survive the cell death period. J Comp Neurol 312:33–42.

Goodyear RJ, Ratnayaka HSK, Warchol ME, Richardson GP. 2014. Staurosporine-induced collapse of cochlear hair bundles. J Comp Neurol 522:3281–3294.

Graus F, Ferrer I. 1990. Analysis of a neuronal antigen (Hu) expression in the developing rat brain detected by autoantibodies from patients with paraneoplastic encephalomyelitis. Neurosci Lett 112:14–18.

Kaneko N, Okano H, Sawamoto K. 2006. Role of the cholinergic system in regulating

survival of newborn neurons in the adult mouse dentate gyrus and olfactory bulb. Genes to Cells 11:1145–1159.

Kawaguchi Y. 1997. Neostriatal cell subtypes and their functional roles. Neurosci Res 27:1–8.

Kawaguchi Y, Wilson CJ, Augood SJ, Emson PC. 1995. Striatal Interneurons - Chemical, Physiological and Morphological Characterization. Trends Neurosci 18:527–535.

Kim KK, Kim YC, Adelstein RS, Kawamoto S. 2011. Fox-3 and PSF interact to activate neural cell-specific alternative splicing. Nucleic Acids Res 39:3064–3078.

Kim Y, Wang W-ZZ, Comte I, Pastrana E, Tran PB, Brown J, Miller RJ, Doetsch F, Molnár Z, Szele FG. 2010. Dopamine stimulation of postnatal murine subventricular zone neurogenesis via the D3 receptor. J Neurochem 114:750–760.

van der Kooy D, Fishell G. 1987. Neuronal birthdate underlies the development of striatal compartments. Brain Res 401:155–161.

Kútna V, Ševc J, Gombalová Z, Matiašová A, Daxnerová Z. 2014. Enigmatic cerebrospinal fluid-contacting neurons arise even after the termination of neurogenesis in the rat spinal cord during embryonic development and retain their immature-like characteristics until adulthood. Acta Histochem 116:278–285.

Lagace DC, Whitman MC, Noonan MA, Ables JL, DeCarolis NA, Arguello AA, Donovan MH, Fischer SJ, Farnbauch LA, Beech RD, DiLeone RJ, Greer CA, Mandyam CD, Eisch AJ. 2007. Dynamic Contribution of Nestin-Expressing Stem Cells to Adult Neurogenesis. J Neurosci 27:12623–12629.

Lim DA, Alvarez-Buylla A. 2016. The Adult Ventricular-Subventricular Zone (V-SVZ) and Olfactory Bulb (OB) Neurogenesis. Cold Spring Harb Perspect Biol 8:1–34.

Liu X, Wang Q, Haydar TF, Bordey A. 2005. Nonsynaptic GABA signaling in postnatal subventricular zone controls proliferation of GFAP-expressing progenitors. Nat Neurosci 8:1179–1187.

Liu Y, Namba T, Liu J, Suzuki R, Shioda S, Seki T. 2010. Glial fibrillary acidic protein-expressing neural progenitors give rise to immature neurons via early intermediate progenitors expressing both glial fibrillary acidic protein and neuronal markers in the adult hippocampus. Neuroscience 166:241–251.

Marchand R, Lajoie L. 1986. Histogenesis of the striopallidal system in the rat. Neurogenesis of its neurons. Neuroscience 17:573–590.

De Marchis S, Temoney S, Erdelyi F, Bovetti S, Bovolin P, Szabo G, Puche AC. 2004. GABAergic phenotypic differentiation of a subpopulation of subventricular derived migrating progenitors. Eur J Neurosci 20:1307–1317.

Marichal N, García G, Radmilovich M, Trujillo-Cenóz O, Russo RE, Trujillo-ceno O, Marichal N, García G, Radmilovich M, Trujillo-Cenóz O, Russo RE. 2009. Enigmatic central canal contacting cells: immature neurons in “standby mode”? J Neurosci 29:10010–

10024.
Marusich MF, Furneaux HM, Henion PD, Weston JA. 1994. Hu neuronal proteins are expressed in proliferating neurogenic cells. J Neurobiol 25:143–155.
Maslov AY, Barone T a, Plunkett RJ, Pruitt SC. 2004. Neural stem cell detection, characterization, and age-related changes in the subventricular zone of mice. J Neurosci 24:1726–1733.
Merkle FT, Fuentealba LC, Sanders TA, Magno L, Kessaris N, Alvarez-Buylla A. 2014. Adult neural stem cells in distinct microdomains generate previously unknown interneuron types. Nat Neurosci 17:207–214.
Merkle FT, Mirzadeh Z, Alvarez-Buylla A. 2007. Mosaic organization of neural stem cells in the adult brain. Science (80- ) 317:381–384.
Mirzadeh Z, Merkle FT, Soriano-Navarro M, Garcia-Verdugo JM, Alvarez-Buylla A. 2008. Neural Stem Cells Confer Unique Pinwheel Architecture to the Ventricular Surface in Neurogenic Regions of the Adult Brain. Cell Stem Cell 3:265–278.
Mohapel P, Leanza G, Kokaia M, Lindvall O. 2005. Forebrain acetylcholine regulates adult hippocampal neurogenesis and learning. Neurobiol Aging 26:939–946.
Moreno-López B, Noval JA, González-Bonet LG, Estrada C. 2000. Morphological bases for a role of nitric oxide in adult neurogenesis. Brain Res 869:244–250.
Moreno-López B, Romero-Grimaldi C, Noval JA, Murillo-Carretero M, Matarredona ER, Estrada C. 2004. Nitric oxide is a physiological inhibitor of neurogenesis in the adult mouse subventricular zone and olfactory bulb. J Neurosci 24:85–95.
Mori T, Wakabayashi T, Hirahara Y, Takamori Y, Koike T, Kurokawa K, Yamada H. 2012. Differential responses of endogenous adult mouse neural precursors to excess neuronal excitation. Eur J Neurosci 36:3184–93.
Mori T, Yuxing Z, Takaki H, Takeuchi M, Iseki K, Hagino S, Kitanaka J, Takemura M, Misawa H, Ikawa M, Okabe M, Wanaka A. 2004. The LIM homeobox gene, L3/Lhx8, is necessary for proper development of basal forebrain cholinergic neurons. Eur J Neurosci 19:3129–3141.
Mullen RJ, Buck CR, Smith AM. 1992. NeuN, a neuronal specific nuclear protein in vertebrates. Development 116:201–211.
Nakamura M, Sato K, Fukaya M, Araishi K, Aiba A, Kano M, Watanabe M. 2004. Signaling complex formation of phospholipase Cβ4 with metabotropic glutamate receptor type 1α and 1,4,5-trisphosphate receptor at the perisynapse and endoplasmic reticulum in the mouse brain. Eur J Neurosci 20:2929–2944.
Nam SC, Kim Y, Dryanovski D, Walker A, Goings G, Woolfrey K, Kang SS, Chu C, Chenn A, Erdelyi F, Szabo G, Hockberger P, Szele FG. 2007. Dynamic features of postnatal subventricular zone cell motility: a two-photon time-lapse study. J Comp Neurol 505:190–208.

Nguyen L, Malgrange B, Breuskin I, Bettendorff L, Moonen G, Belachew S, Rigo J-M. 2003. Autocrine/paracrine activation of the GABA(A) receptor inhibits the proliferation of neurogenic polysialylated neural cell adhesion molecule-positive (PSA-NCAM+) precursor cells from postnatal striatum. J Neurosci 23:3278–3294.

O'Keeffe GC, Barker RA, Caldwell MA. 2009. Dopaminergic modulation of neurogenesis in the subventricular zone of the adult brain. Cell Cycle 8:2888–2894.

Oga T, Elston GN, Fujita I. 2017. Postnatal Dendritic Growth and Spinogenesis of Layer-V Pyramidal Cells Differ between Visual, Inferotemporal, and Prefrontal Cortex of the Macaque Monkey. Front Neurosci 11:118.

Okano HJ, Darnell RB. 1997. A hierarchy of Hu RNA binding proteins in developing and adult neurons. J Neurosci 17:3024–3037.

Orts-Del'Immagine A, Seddik R, Tell F, Airault C, Er-Raoui G, Najimi M, Trouslard J, Wanaverbecq N. 2016. A single polycystic kidney disease 2-like 1 channel opening acts as a spike generator in cerebrospinal fluid-contacting neurons of adult mouse brainstem. Neuropharmacology 101:549–565.

Ouimet CC, Langley-Gullion KC, Greengard P. 1998. Quantitative immunocytochemistry of DARPP-32-expressing neurons in the rat caudatoputamen. Brain Res 808:8–12.

Paez-Gonzalez P, Asrican B, Rodriguez E, Kuo CT. 2014. Identification of distinct $ChAT^{+}$ neurons and activity-dependent control of postnatal SVZ neurogenesis. Nat Neurosci 17:934–942.

Paxinos G, Franklin KBJ. 2001. The mouse brain in stereotaxic coordinates, 2nd edn. San Diego: Academic Press.

Platel J-C, Heintz T, Young S, Gordon V, Bordey A. 2008. Tonic activation of GLUK5 kainate receptors decreases neuroblast migration in whole-mounts of the subventricular zone. J Physiol 586:3783–3793.

Reiner A, Perera M, Paullus R, Medina L. 1998. Immunohistochemical localization of DARPP32 in striatal projection neurons and striatal interneurons in pigeons. J Chem Neuroanat 16:17–33.

Romero-Grimaldi C, Moreno-López B, Estrada C. 2008. Age-dependent effect of nitric oxide on subventricular zone and olfactory bulb neural precursor proliferation. J Comp Neurol 506:339–346.

Sarnat HB, Nochlin D, Born DE. 1998. Neuronal nuclear antigen (NeuN): a marker of neuronal maturation in early human fetal nervous system. Brain Dev 20:88–94.

Sato T. 1968. A modified method for lead staining of thin sections. J Electron Microsc (Tokyo) 17:158–159.

Sawamoto K, Wichterle H, Gonzalez-Perez O, Cholfin J a, Yamada M, Spassky N, Murcia NS, Garcia-Verdugo JM, Marin O, Rubenstein JLR, Tessier-Lavigne M, Okano H, Alvarez-Buylla A. 2006. New neurons follow the flow of cerebrospinal fluid in the adult

brain. Science 311:629–632.
Seki T. 2002. Expression patterns of immature neuronal markers PSA-NCAM, CRMP-4 and NeuroD in the hippocampus of young adult and aged rodents. J Neurosci Res 70:327–334.
Takamori Y, Wakabayashi T, Mori T, Kosaka J, Yamada H. 2014. Organization and cellular arrangement of two neurogenic regions in the adult ferret (Mustela putorius furo) brain. J Comp Neurol 522:1818–1838.
Tamamaki N, Yanagawa Y, Tomioka R, Miyazaki JI, Obata K, Kaneko T. 2003. Green Fluorescent Protein Expression and Colocalization with Calretinin, Parvalbumin, and Somatostatin in the GAD67-GFP Knock-In Mouse. J Comp Neurol 467:60–79.
Tong CK, Chen J, Cebrián-Silla A, Mirzadeh Z, Obernier K, Guinto CD, Tecott LH, García-Verdugo JM, Kriegstein A, Alvarez-Buylla A. 2014. Axonal control of the adult neural stem cell niche. Cell Stem Cell 14:500–511.
Vígh B, Manzano e Silva MJ, Frank CL, Vincze C, Czirok SJ, Szabó A, Lukáts A, Szél A. 2004. The system of cerebrospinal fluid-contacting neurons. Its supposed role in the nonsynaptic signal transmission of the brain. Histol Histopathol 19:607–628.
Wang F, Tidei JJ, Polich ED, Gao Y, Zhao H, Perrone-Bizzozero NI, Guo W, Zhao X. 2015. Positive feedback between RNA-binding protein HuD and transcription factor SATB1 promotes neurogenesis. Proc Natl Acad Sci U S A 112:E4995–E5004.
Wright J, Stanic D, Thompson LH. 2013. Generation of striatal projection neurons extends into the neonatal period in the rat brain. J Physiol 591:67–76.
Young SZ, Lafourcade CA, Platel J, Lin T V, Bordey A. 2014. GABAergic striatal neurons project dendrites and axons into the postnatal subventricular zone leading to calcium activity. Front Cell Neurosci 8:10.
Young SZ, Taylor MM, Bordey A. 2011. Neurotransmitters couple brain activity to subventricular zone neurogenesis. Eur J Neurosci 33:1123–1132.

Figure legends

Fig.1.

NeuN+ cells in the adult SVZ (SVZ-Ns). (A) Schematic representation of single optical confocal microscopy images. (B) Mature SVZ-Ns (M-SVZ-Ns) localized in the SVZ (arrows) with typical neuronal nuclear morphology. Small SVZ-Ns (S-SVZ-Ns) localized in the dorsal (C) and ventral (D) part of the SVZ. Both dorsal S-SVZ-Ns (DS-SVZ-Ns) and ventral S-SVZ-Ns (VS-SVZ-Ns) had small nuclei and expressed DCX (arrows in C and D). M-SVZ-Ns did not express DCX and were scattered throughout the SVZ (arrowheads in C and D). There were NeuN+ cells contacting the SVZ (open arrowheads in B and D), but we excluded these cells from our analysis. (E) Nuclear volume of M-SVZ-Ns was significantly larger than that of DS/VS-SVZ-Ns. (F) Nuclear shape of DS-SVZ-Ns was significantly elongated. Total 15-20 cells from 3 mice were analyzed in each group. Dotted line, outline of the SVZ; cc, corpus callosum; CPu, caudate putamen; Sep, septum; ns, not significant; *, $p < 0.05$; **, $p < 0.01$. Scale bar = 20 μm.

Fig. 2.

SVZ-Ns in the adult and early postnatal brain. GFAP+ (A) and EGFR+ (B) processes enwrapped M-SVZ-Ns (arrowheads). (C) M-SVZ-Ns were also detected in the caudal SVZ (arrows). Images were taken from a section at -0.8 mm posterior from the bregma (boxed area). In the postnatal one week brain, M-SVZ-Ns without expressing DCX (D, arrowhead) and S-SVZ-Ns expressing DCX (E, arrows) were detected. Note that the SVZ is very thick in the early postnatal brain. Single optical confocal microscope images are shown. fi, fimbria of the hippocampus. Scale bar = 20 μm.

Fig. 3.

Neuronal marker expressions in M-SVZ-Ns. (A) Average number of M-SVZ-Ns per section was significantly larger than that of HuC/D+ M-SVZ-Ns. (B) Single optical confocal microscopy images showing HuC/D expression both in the Sox2- M-SVZ-Ns with large nuclei (arrow) and the Sox2+ NPCs with small nuclei (arrowheads). Note that HuC/D localized in the nuclei of mature neurons including striatal neurons (open arrowhead), but localized in the cytoplasm of NPCs. (C) Virtually all HuC/D+ cells were NeuN+ (arrow), but there were many NeuN+/HuC/D- cells in the SVZ (arrowheads) and striatum. Single optical confocal microscopy images are shown. (D) Quantification of marker expressing M-SVZ-Ns. n = 3 mice in each group. (E-J) Single optical confocal microscopy images of M-SVZ-Ns expressing markers. In each merged image, a Hoechst33258 nuclear image was added. Majority of M-SVZ-Ns expressed GAD67 (GFP in GAD67-GFP mice, E) and DARPP-32 (F). Small number of M-SVZ-Ns expressed nNOS (G), Calretinin (CR, H), or Parvalbumin (PV, I).

(J) ChAT+ M-SVZ-Ns were extremely rare. In some cases, the processes of M-SVZ-Ns were revealed (arrowheads in G, I, J). Scale bar = 20 μm.

Fig. 4.
Birth date analysis of M-SVZ-Ns. (A) M-SVZ-Ns were generated with peaks at E13 and P1. White bars indicate the ratio of BrdU+ cells among M-SVZ-Ns (NeuN+ cells in the SVZ) (left axis). Black bars indicate the average number of BrdU+/NeuN+ cells in the SVZ per section (right axis). (B) Neurogenesis in the striatum. Vast majority of striatal neurons were generated during embryonic stages. The densities of NeuN+/BrdU+ cells in the striatum are indicated. (C) Single optical confocal microscopy images of a BrdU+ M-SVZ-N (arrow). BrdU was injected at P1 and analyzed at the adult stage. In the merged image, a Hoechst33258 nuclear image was added. n = 3 in each group. Scale bar = 20 μm.

Fig. 5.
Morphology and axonal target of M-SVZ-Ns. To visualize the entire morphology, Lucifer Yellow (LY) was injected. (A, B) Stacked confocal microscopy images representing typical M-SVZ-Ns. Left and right panels indicate LY and merged images of LY and Hoechst33258, respectively. Inset images show single optical confocal microscopy images indicating the position of cell bodies in the SVZ (arrows). The surface of the SVZ made a steep (A) or gentle (B) slope in each section. Many processes of the M-SVZ-N extended almost parallel to the SVZ. Note that, some processes extended among NPCs (arrowheads). (C) The same cell presented in B is shown as a 3D image from the diagonal view point. A process ran in the SVZ (arrowheads). The striatal neurons radially extended their processes (inset). (D) An electron microscopy image of a M-SVZ-N. After NeuN immunohistochemistry, electron microscopy analysis was performed (boxed area). The M-SVZ-N (arrow) was covered by ependymal cells. (E) Single optical confocal microscopy images showing M-SVZ-Ns that were retrogradely labeled by FluoroGold (FG, arrow). FG was injected into the substantia nigra. In the merged image, a propidium iodide (PI) nuclear image was added. E, ependymal cell. Scale bar in A, D, E = 20, 5, 20 μm, respectively.

Fig. 6.
Characterization of S-SVZ-Ns. Both DS-SVZ-Ns (A, C) and VS-SVZ-Ns (B, D) expressed Sox2 (A, B) and MCM2 (C, D). Arrows indicate double + cells. Single optical confocal microscopy images are shown. Scale bar = 20 μm.

Fig. 7.
Migration of S-SVZ-Ns. (A) Small number of S-SVZ-Ns expressing DCX in the SVZ incorporated BrdU three hours after the last injection of BrdU (arrow). At that time, there

were many BrdU+ cells in the SVZ (A), but few BrdU+ cells in the OB (B, arrowhead). In the merged image of panel B, a Hoechst33258 image was added. (C) Many BrdU+/DCX+ S-SVZ-Ns in the OB were detected seven days after the last injection of BrdU (arrows). Single optical confocal microscopy images are shown. core, core of the OB; GCL, granule cell layer of the OB. Scale bars = 20 μm.

Fig. 8.
Differential expression of GAD67 in DS/VS-SVZ-Ns. DS-SVZ-Ns did not express GFP (A, arrowheads), but VS-SVZ-Ns expressed GFP (B, arrows) in GAD67-GFP mice. DCX-M-SVZ-Ns were GFP+ (A, open arrowhead). (C) In the RMS, both NeuN+/DCX+/GFP+ (arrows) and NeuN+/DCX+/GFP- (arrowhead) cells were detected. (D) In the OB, all NeuN+/DCX+ cells were GFP+ (arrows). Single optical confocal microscopy images are shown. Scale bar = 20 μm.

Fig. 9.
S-SVZ-Ns did not undergo apoptosis. (A) In the anterior tip of the SVZ and RMS, activated Caspase-3 (Cas3)+ cells were NeuN- (arrowhead), while NeuN+ S-SVZ-Ns were Cas3- (open arrowhead). Single optical confocal microscopy images are shown. (B) An electron microscopy image of an S-SVZ-N. Co-localization of NeuN and DCX was confirmed with a confocal microscope (white arrows), and this cell was processed for electron microscopy analysis. Note that S-SVZ-N had scant cytoplasm (black arrows) and lax chromatin. Scale bar in A, B = 20, 1 μm, respectively.

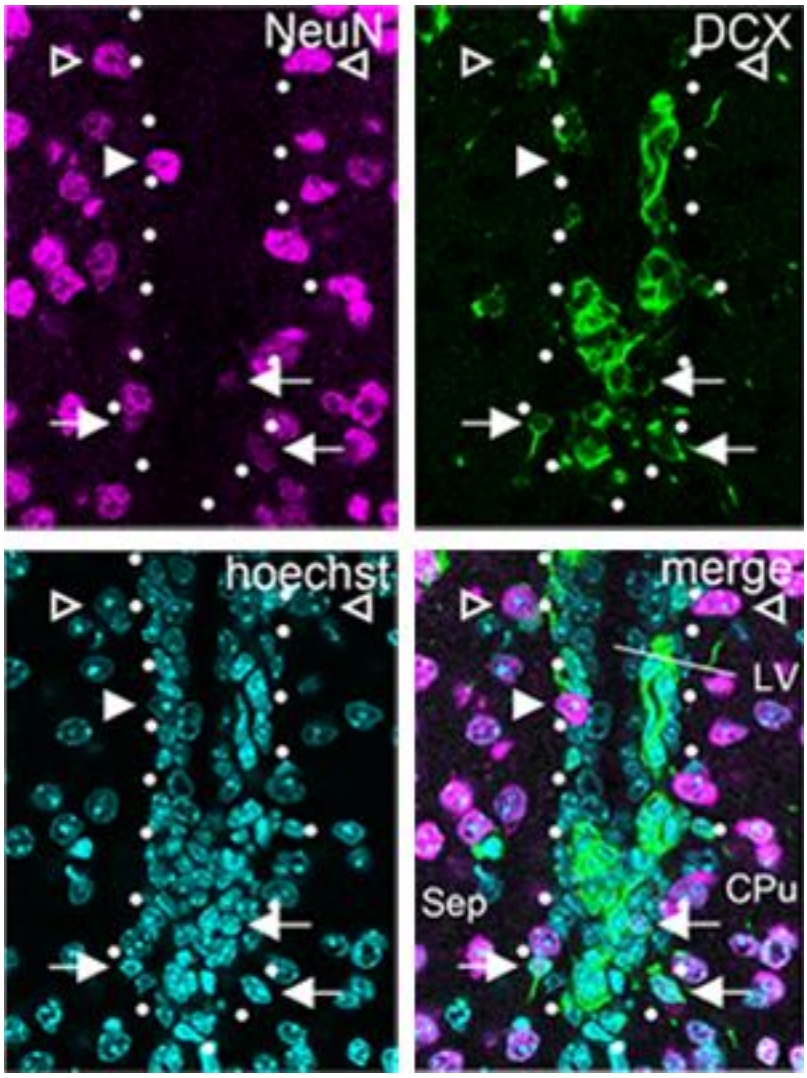


Graphical abstract

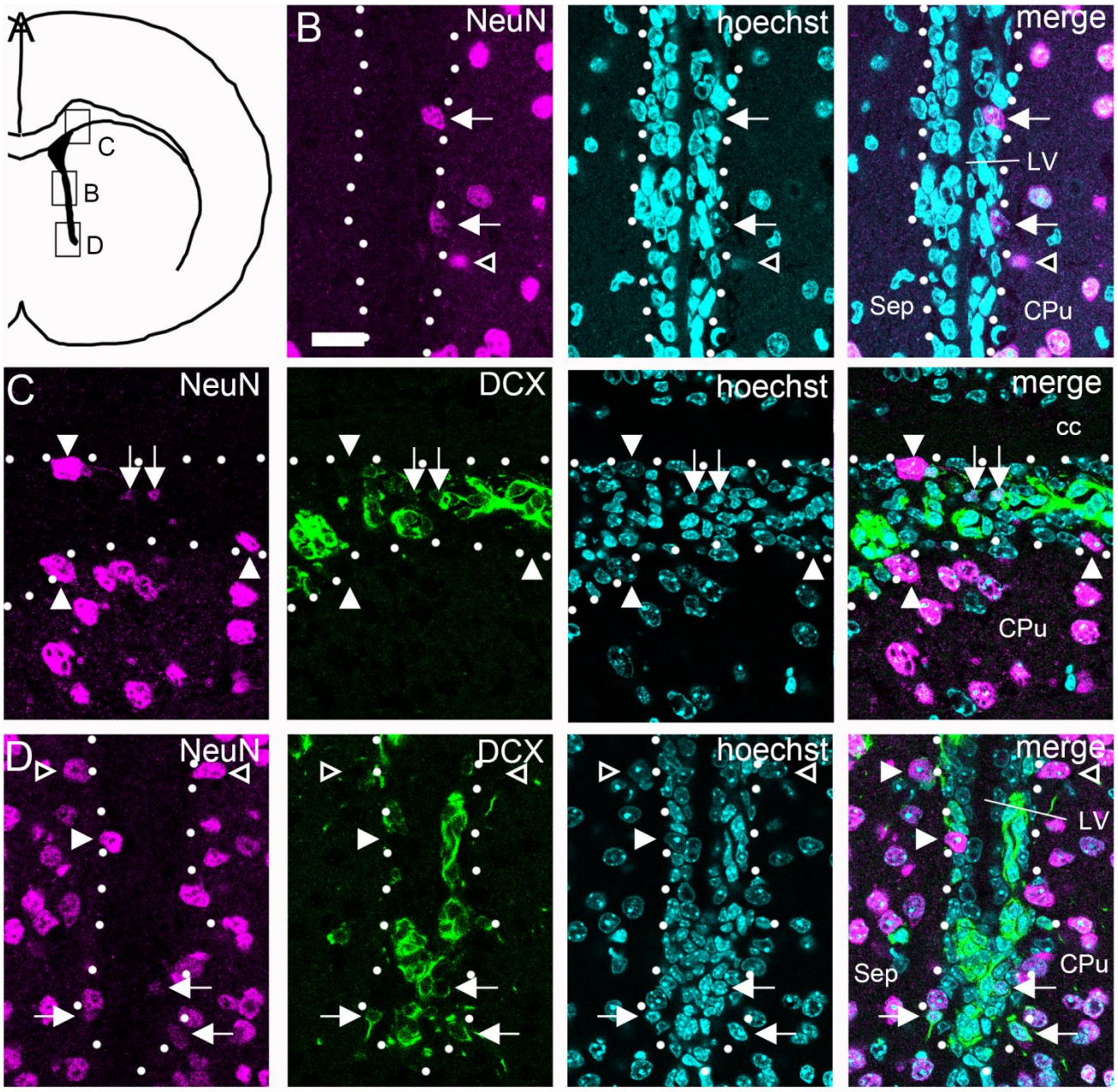
A
C
B
D
B
NeuN
hoechst
merge
LV
Sep
CPu
C
NeuN
DCX
hoechst
merge
cc
CPu
D
NeuN
DCX
hoechst
merge
LV
Sep
CPu

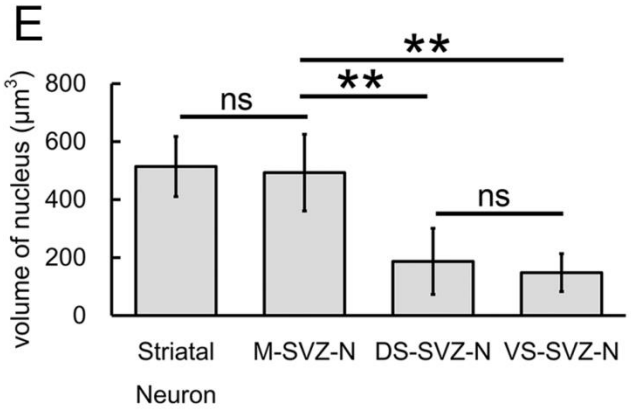
E
volume of nucleus (μm3)
800
600
400
200
0
ns
**
**
ns
Striatal Neuron
M-SVZ-N
DS-SVZ-N
VS-SVZ-N

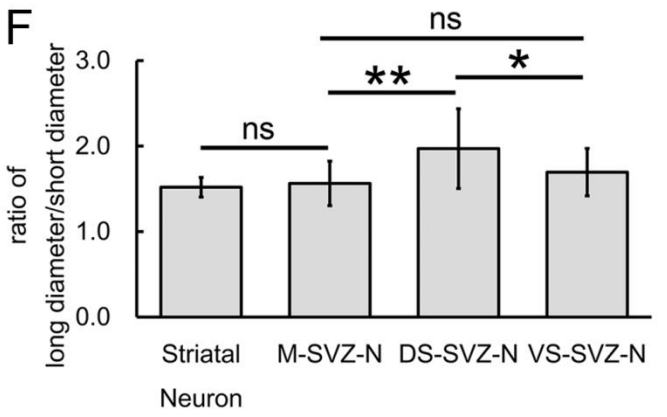
F
ratio of long diameter/short diameter
3.0
2.0
1.0
0.0
ns
**
*
ns
Striatal Neuron
M-SVZ-N
DS-SVZ-N
VS-SVZ-N

Fig. 1

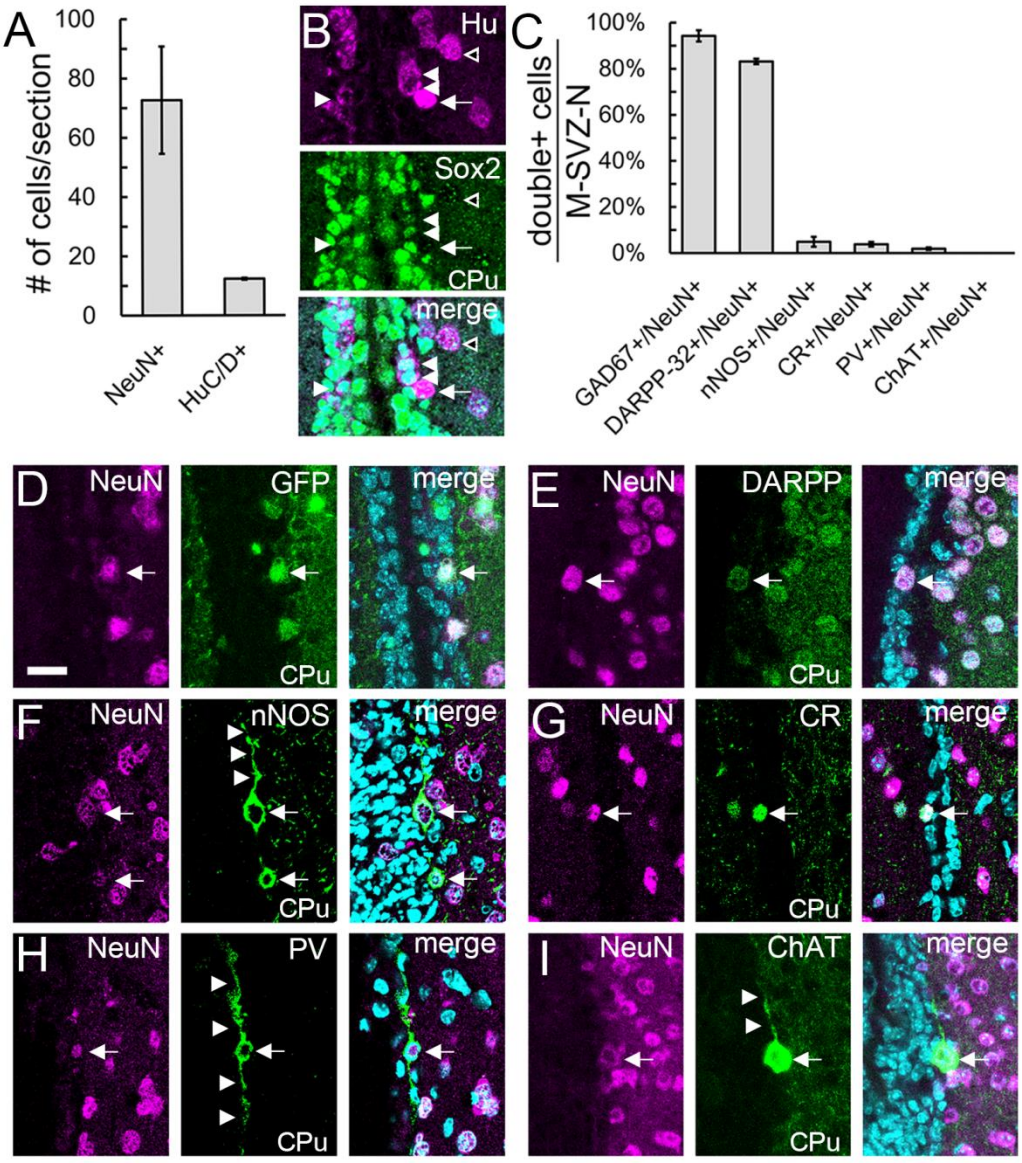
A
# of cells/section
100
80
60
40
20
0
NeuN+
HuC/D+
B
Hu
Sox2
CPu
merge
C
double+ cells
M-SVZ-N
100%
80%
60%
40%
20%
0%
GAD67+/NeuN+
DARPP-32+/NeuN+
nNOS+/NeuN+
CR+/NeuN+
PV+/NeuN+
ChAT+/NeuN+
D
NeuN
GFP
merge
CPu
E
NeuN
DARPP
merge
CPu
F
NeuN
nNOS
merge
CPu
G
NeuN
CR
merge
CPu
H
NeuN
PV
merge
CPu
I
NeuN
ChAT
merge
CPu

Fig. 2

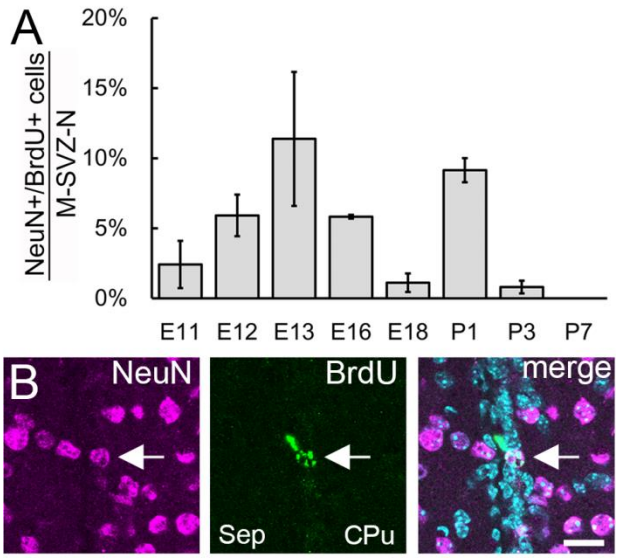
A
NeuN+/BrdU+ cells
M-SVZ-N
20%
15%
10%
5%
0%
E11
E12
E13
E16
E18
P1
P3
P7
B
NeuN
BrdU
merge
Sep
CPu

Fig. 3

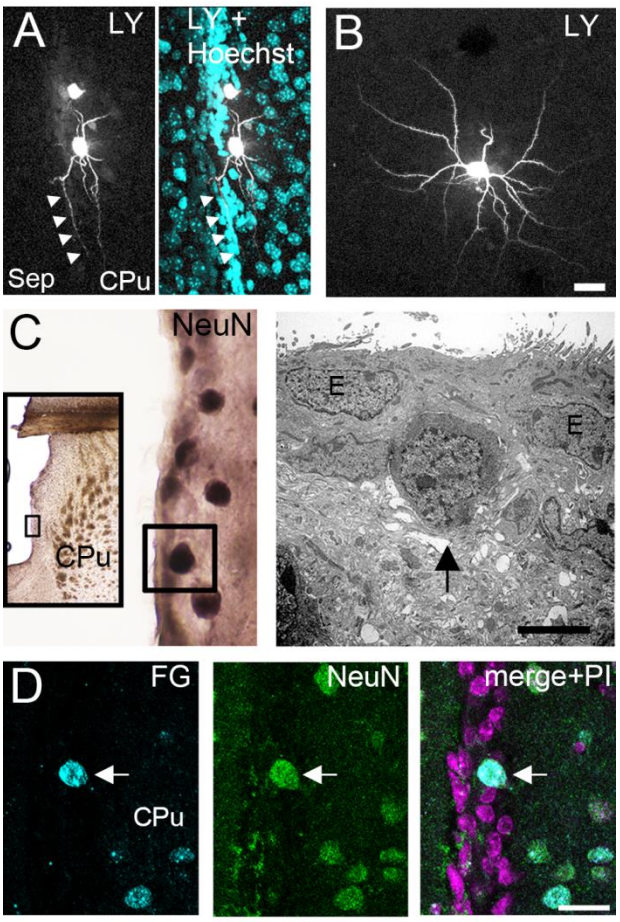


Fig. 4

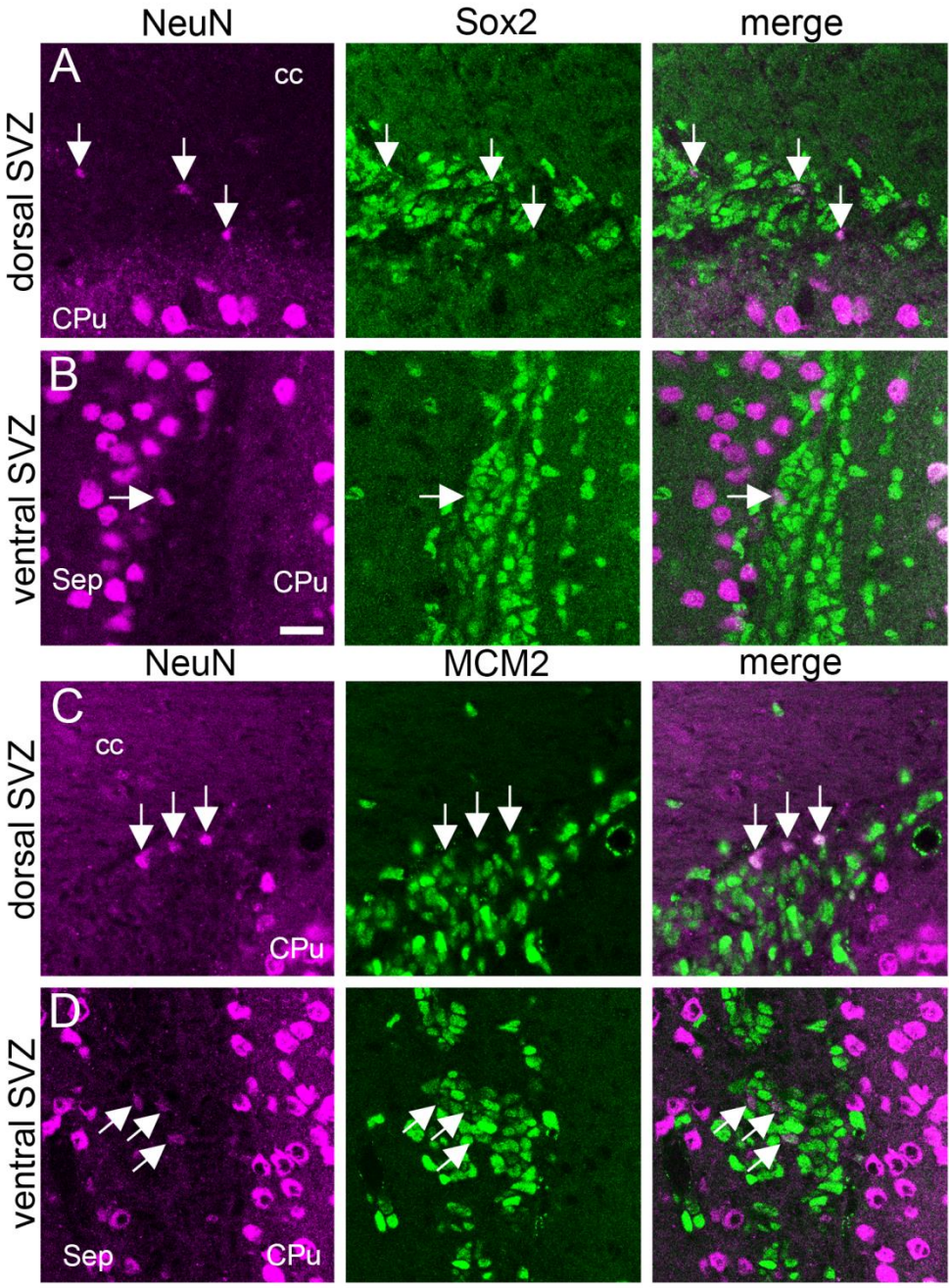
NeuN
Sox2
merge
A
cc
dorsal SVZ
CPu
B
ventral SVZ
Sep
CPu
NeuN
MCM2
merge
C
cc
dorsal SVZ
CPu
D
ventral SVZ
Sep
CPu

Fig. 5

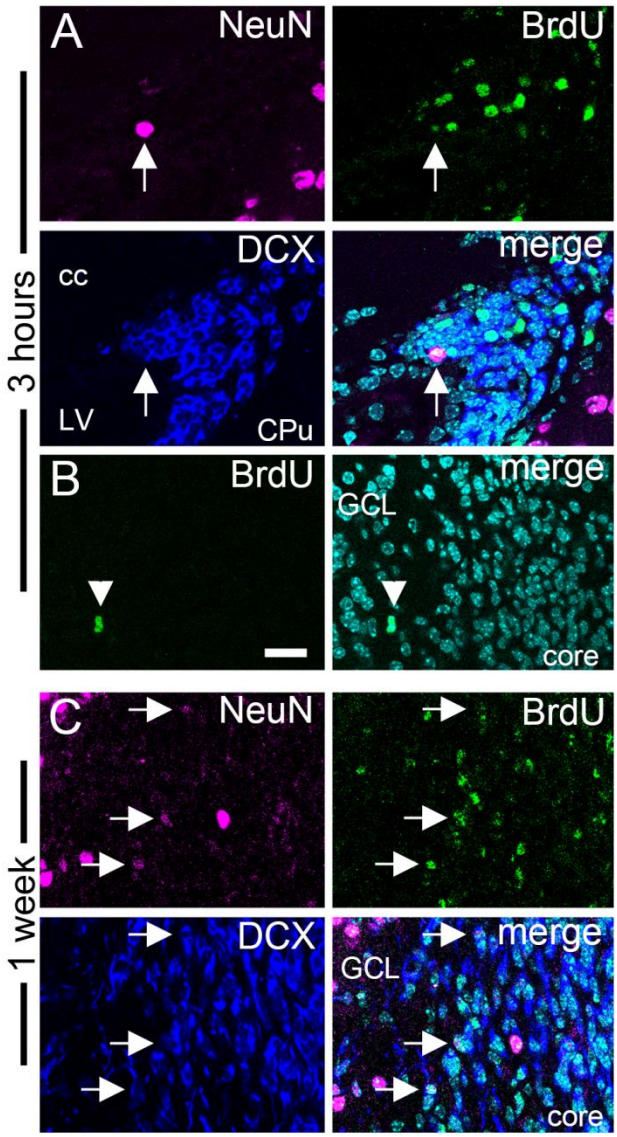
A
NeuN
BrdU
DCX
merge
cc
LV
CPu
3 hours
B
BrdU
merge
GCL
core
C
NeuN
BrdU
DCX
merge
GCL
core
1 week

Fig. 6

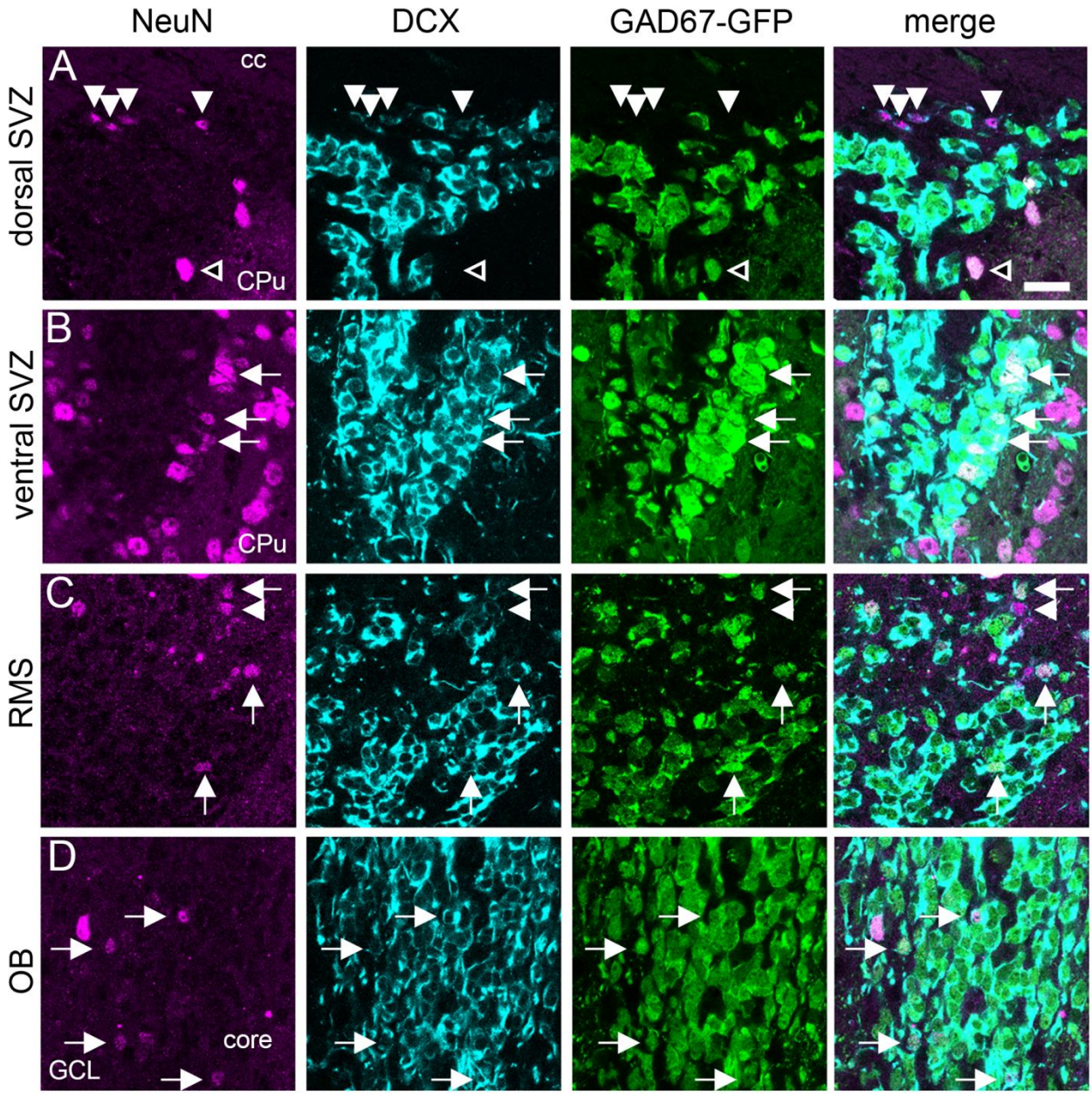
NeuN
DCX
GAD67-GFP
merge
A
cc
CPu
dorsal SVZ
B
CPu
ventral SVZ
C
RMS
D
core
GCL
OB

Fig. 7

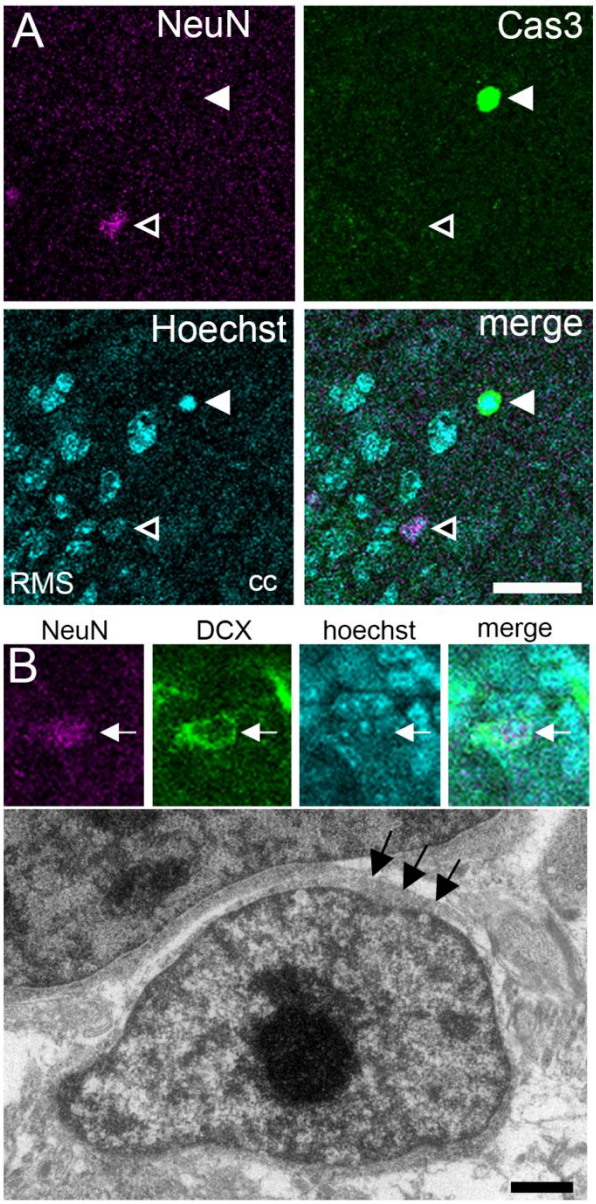


Fig. 8

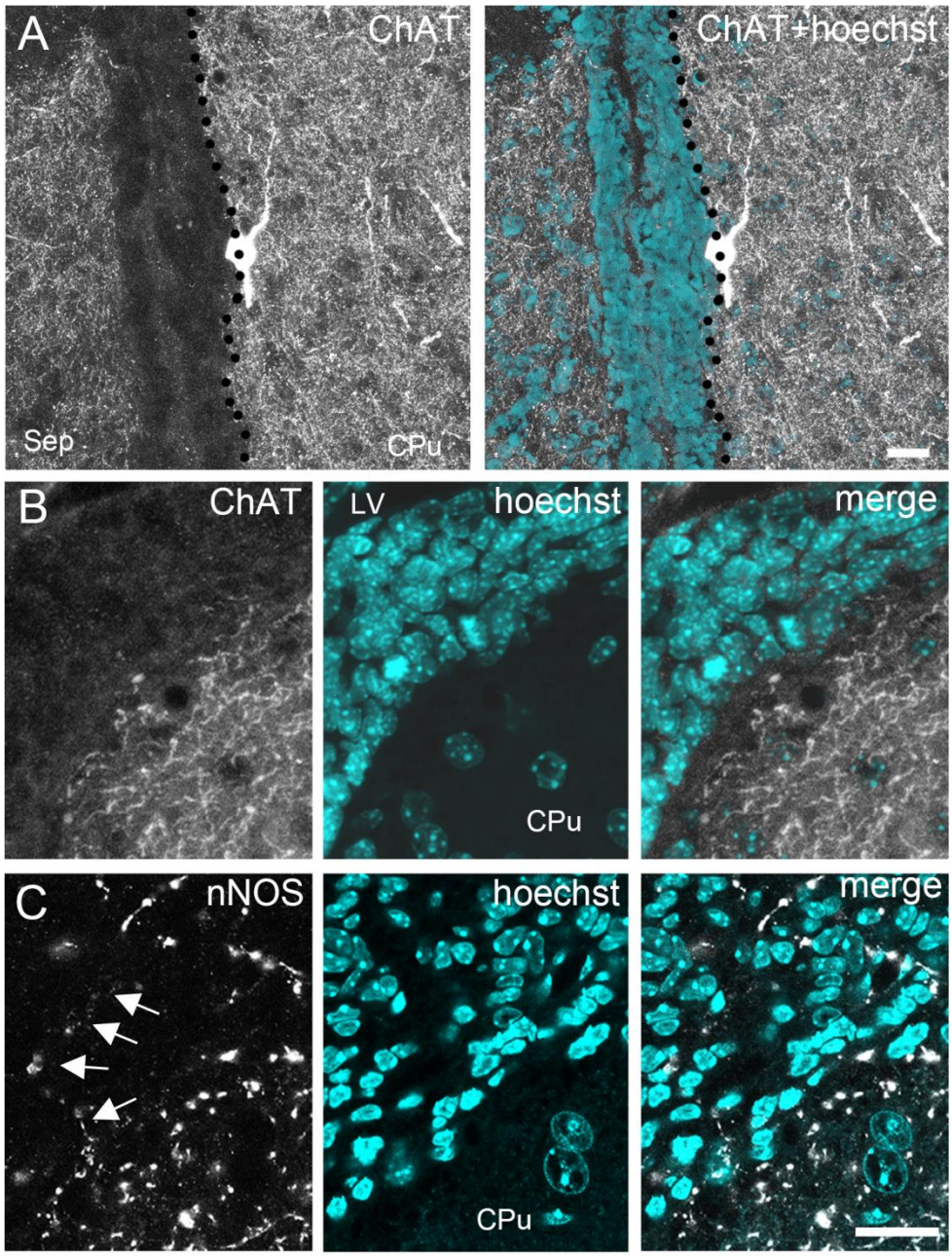


Supplemental Fig. 1

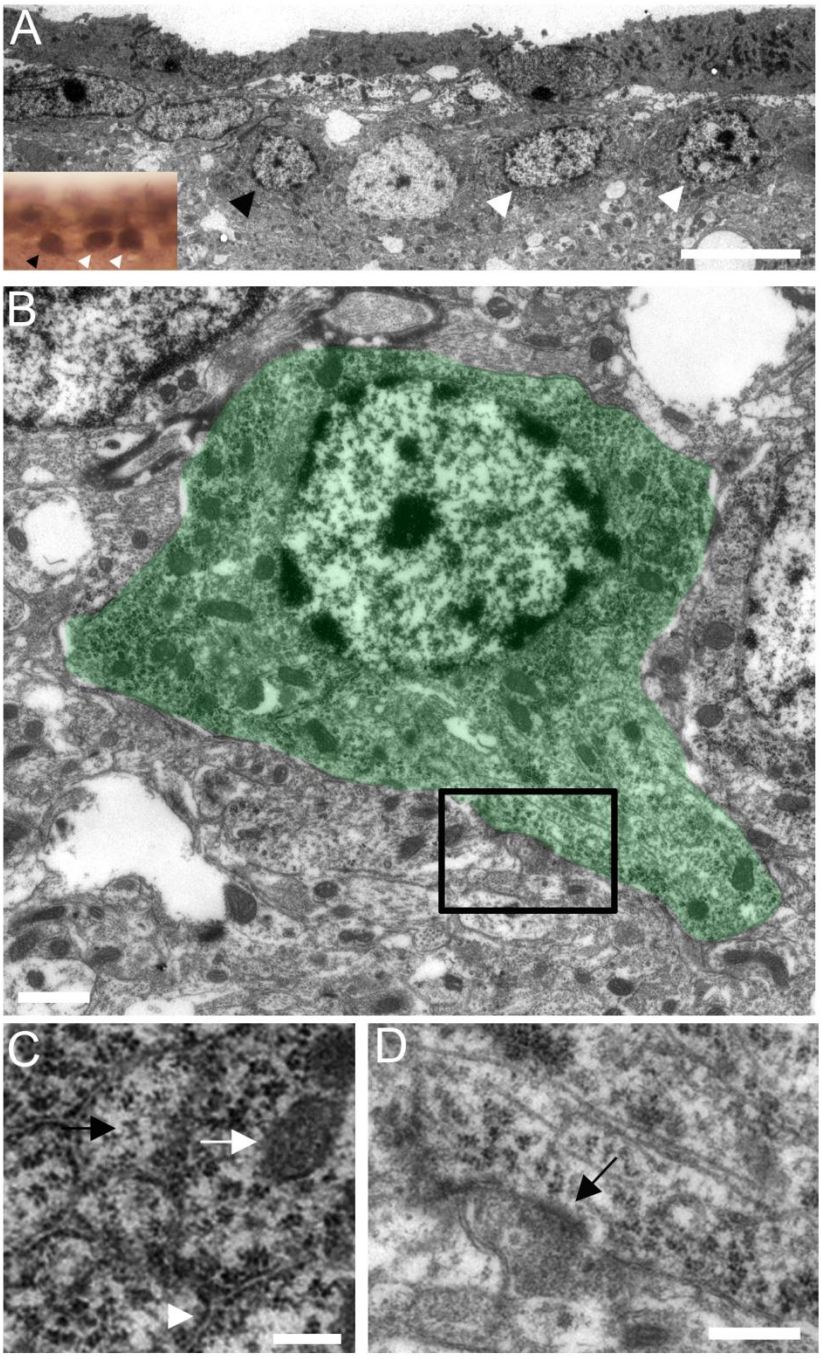


Supplemental Fig. 2

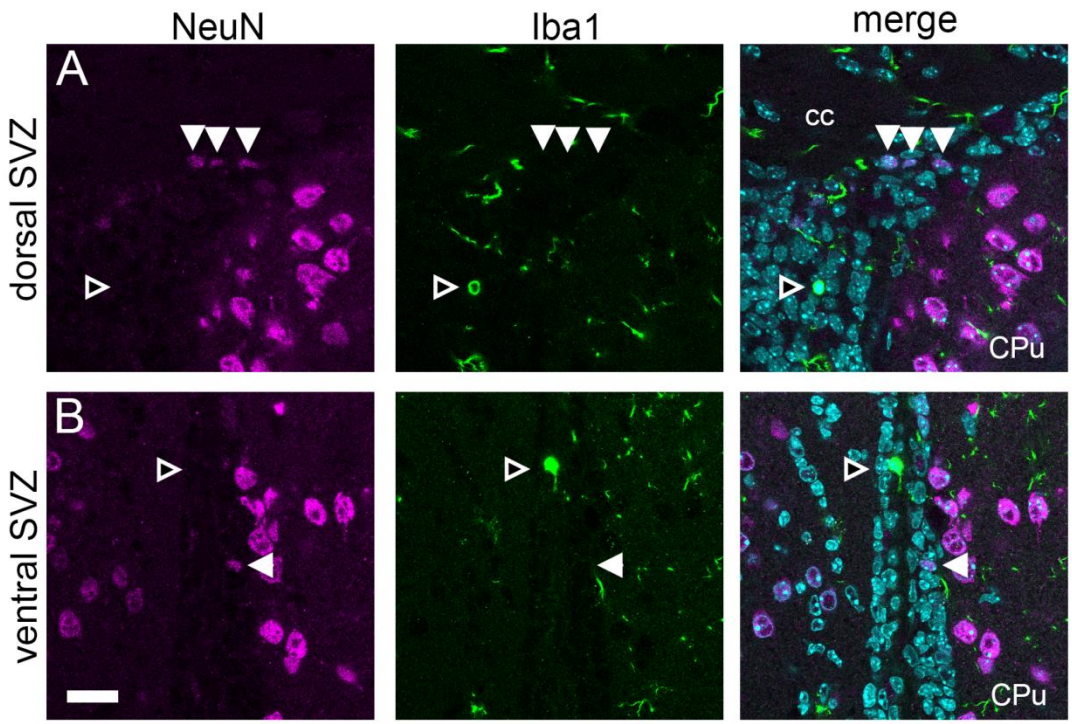


Supplemental Fig. 3

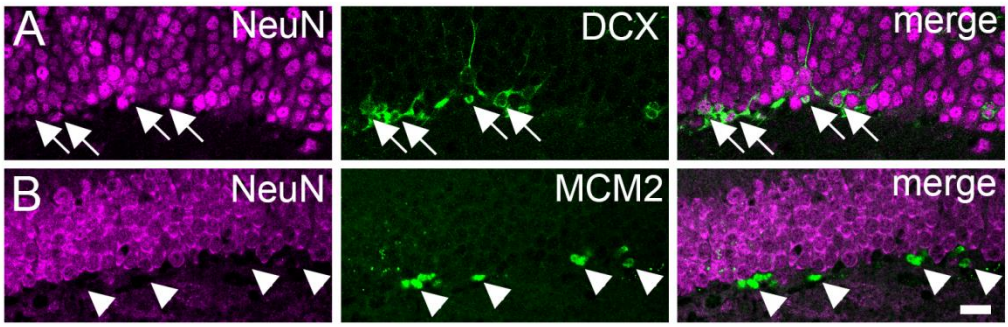


Supplemental Fig. 4